Broadband Upgrade for the 1.668-GHz (L-Band) Radio Astronomy Feed System on the DSN 70-m Antennas

Daniel J. Hoppe,* Behrouz Khayatian,* Bernardo Lopez,* Troy Torrez,* Ezra Long,* John Sosnowski,* Manuel Franco,* and Larry Teitelbaum†

ABSTRACT. — Currently, each of the three Deep Space Network (DSN) 70-m antennas provides a narrowband, 1.668-GHz (L-band) receive capability for radio astronomy observations. This capability is delivered by a large feedhorn mounted on the exterior of one of the feedcones. It provides a single polarization into a pair of redundant low-noise amplifiers. Recently, funding was obtained to upgrade this system to wideband (1.4–1.9 GHz) dual-polarization operation. This required development of a new feedhorn, polarizer, orthomode transducer (OMT), and waveguide transitions. In this article, we describe the design and laboratory testing of these components.

I. Introduction

In 1985, a narrowband, 1.668-GHz (L-band) feed system was installed on all three then-64-m Deep Space Network (DSN) antennas at the Goldstone, Canberra, and Madrid Deep Space Communications Complexes to provide tracking support for the international Vega missions to Venus, which included flybys of Halley's comet [1]. Figure 1 is an image of the existing L-band feed system on DSS-14, now the 70-m-diameter antenna at Goldstone.

In this article, we describe a broadband upgrade for this system. With this upgrade, wideband feed systems operating at approximately 1.7 GHz on two of the DSN 70-m antennas acting as radio telescopes will be capable of high-accuracy pulse time-of-arrival (TOA) measurements of natural emission from millisecond radio pulsars.

Millisecond pulsars (MSPs) are a class of radio pulsars with extremely stable rotations. Precise timing of an array of such pulsars widely distributed on the sky will potentially be the first method to directly detect low-frequency gravitational waves. Effectively, a gravitational wave passing over the Earth produces a systematic advance or delay in the arrival times of pulses from pulsars in the same general area on the sky, a technique ("pulsar timing array")

* Communications Ground Systems Section.
† DSN/Mission Services Planning and Management Program Office.

The research described in this publication was carried out by the Jet Propulsion Laboratory, California Institute of Technology, under a contract with the National Aeronautics and Space Administration.

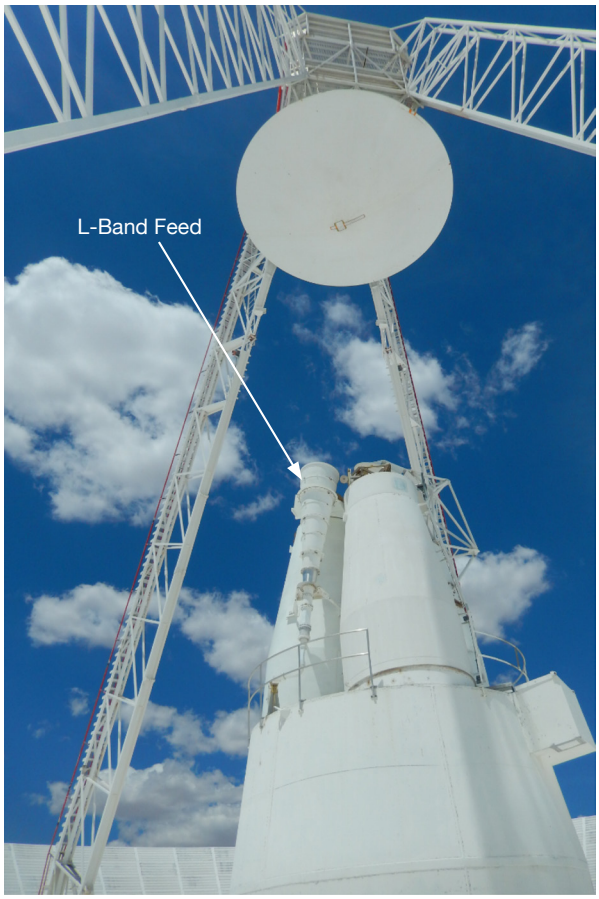

Figure 1. Photo of the existing L-band feed system on the 70-m antenna at Goldstone (DSS-14), in an "outrigger" position in the tri-cone system at the Cassegrain focus.

pioneered at JPL by Hellings and Downs [2]. Properly instrumented, and making opportunistic use of DSN schedule gaps for these pulsar observations, DSN antennas should be capable of obtaining the high timing accuracy required for the direct detection of gravitational radiation.

The existing system's block diagram and the block diagram appropriate for the upgrade discussed here are shown in Figures 2 and 3, respectively. As shown in Figure 2, the existing system employs a smooth-walled Potter horn, a narrowband polarizer, and a redundant set of low-noise amplifiers (LNAs), either of which can be selected by a WR430 waveguide switch. This system is optimized at 1.668 GHz and provides a single polarization at the output.

In order to obtain an operating bandwidth of 1.4–1.9 GHz, it is necessary to replace the narrowband Potter horn with a wideband corrugated horn. In addition, the polarizer must be replaced with a broadband design. Finally, to provide simultaneous access to both polarizations (left-handed [LCP] and right-handed [RCP]), we use an orthomode transducer (OMT). This three-port device (two WR430 ports and one circular waveguide port) excites an x-polarized $TE_{1,1}$ circular mode in the common circular waveguide port through one of its WR430 ports and a y-polarized $TE_{1,1}$ circular waveguide mode through a second WR430

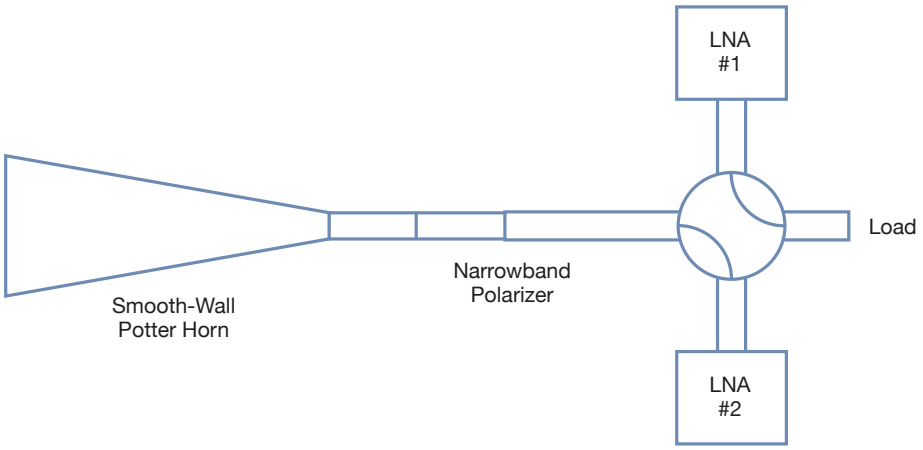

Figure 2. 70-m L-band feed system block diagram (existing).

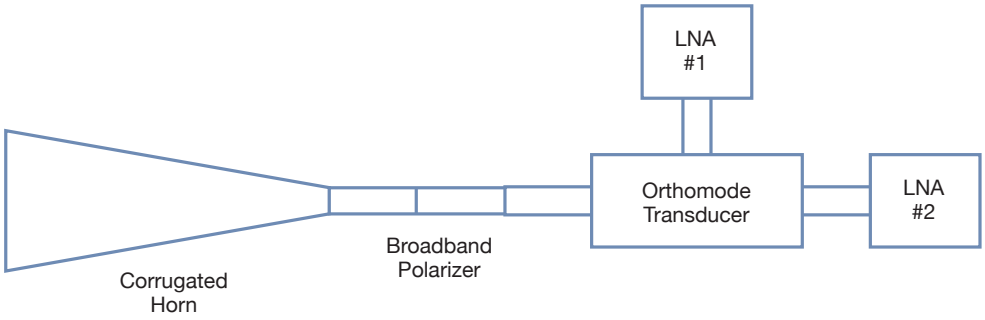

Figure 3. 70-m L-band feed system block diagram (upgraded).

port. These x- and y–polarized $TE_{1,1}$ modes are transformed into RCP and LCP modes by the polarizer. In this manner, the LNAs' inputs represent RCP and LCP components on the sky.

In the next section, we summarize the performance of the existing system over the required 1.4–1.9 GHz band, providing the motivation for the new feedhorn, polarizer, and orthomode designs.

II. Existing L-Band System Performance

In this section, we review the performance of the existing L-band system. The bandwidth of this system is determined by the ability of the smooth-walled Potter horn to provide high-quality illumination of the 70-m subreflector, and by the polarization purity provided by the polarizer. Both of these components are in fact quite limited in bandwidth and both need to be replaced to achieve 1.4–1.9 GHz operation. In addition, as described earlier, in order to achieve simultaneous dual polarization, we need to develop a new OMT for this application. We will discuss these new component designs in the following section.

The existing L-band feed is a Potter horn design [3], which is a smooth-walled horn that employs a simple step to excite both the $TE_{1,1}$ and $TM_{1,1}$ waveguide modes and a drift section to phase these modes appropriately in the horn aperture. This type of horn is a good choice for the original L-band narrowband application since it provides a radiation pattern nearly identical to a corrugated horn (equal E- and H-plane beamwidths, and low sidelobes). Since it is smooth-walled, it can have low mass and can be fabricated using low-cost techniques, key factors for this low frequency of operation and correspondingly large dimensions.

Figures 4–6 show the computed radiation pattern of the existing L-band horn at the design frequency of 1.668 GHz, and at the proposed band edges, 1.4 and 1.9 GHz. As expected, an excellent pattern is obtained at the design frequency, but poor performance is seen at the band edges, where the E- and H-plane patterns are unequal, and sidelobes increase.

While visual inspection of the horn patterns themselves shows significant degradation across the 1.4–1.9 GHz band, ultimately we are concerned with the overall performance of the dual-reflector antenna. This quantity is best expressed as the overall antenna efficiency, η_{dB}, which is a ratio of the achieved antenna gain relative to the available gain,

$$\eta_{\mathrm{dB}} = -10 \log 10\left(\frac{G}{Gmax}\right)$$

with

$$Gmax = \left(\frac{\pi D}{\lambda}\right)^2.$$

Note that here we have chosen to use a minus sign in the definition of the efficiency in dB. In this way, an efficiency of +3 dB implies that the gain is 50 percent of the achievable gain.

Figure 7 plots the computed 70-m antenna efficiency as a function of frequency, using the existing Potter horn. Three factors affecting the gain are included: spillover past the subreflector, spillover past the main reflector, and loss due to the feed pattern phase and amplitude distribution that illuminates the secondary. Spillover past the primary is nearly constant and well-controlled, but spillover past the secondary becomes non-negligible as we move away from the design frequency of 1.668 GHz. The feed amplitude and phase patterns degrade significantly away from 1.668 GHz, and contribute 3 dB of loss alone at 1.9 GHz. Phrased another way, at 1.9 GHz, using the existing feed, the 70-m antenna is operating at the level of a well-illuminated 44-m-diameter antenna. For comparison, a typical corrugated horn can achieve an efficiency on a par with the best Potter horn efficiency (0.5 dB), across the entire 1.4–1.9 GHz band.

Polarization purity is also a significant factor for many science and communication applications. For this L-band system, the operating polarization is fixed circular, either LCP or RCP. Most polarizers are realized in a circular waveguide that supports two orthogonal linear polarizations. By delaying or advancing one of these linearly polarized waves by 90 deg with respect to the other, RCP or LCP will result at the polarizer's output. The frequency range over which this 90-deg difference is maintained determines the polarizer bandwidth.

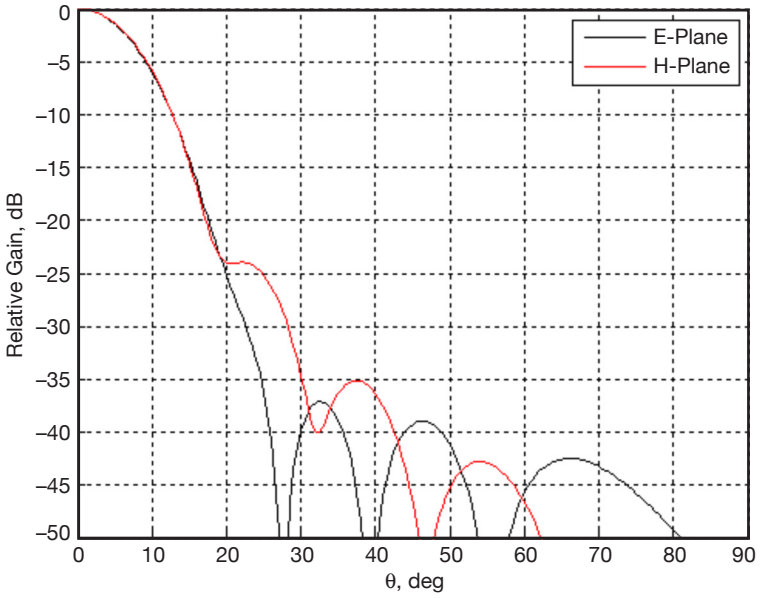

Figure 4. Existing L-band feedhorn pattern at 1.668 GHz.

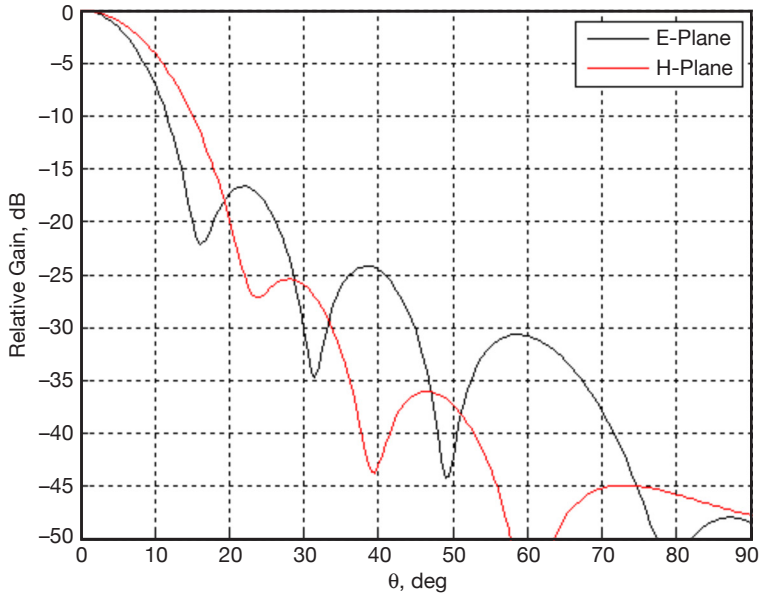

Figure 5. Existing L-band feedhorn pattern at 1.4 GHz.

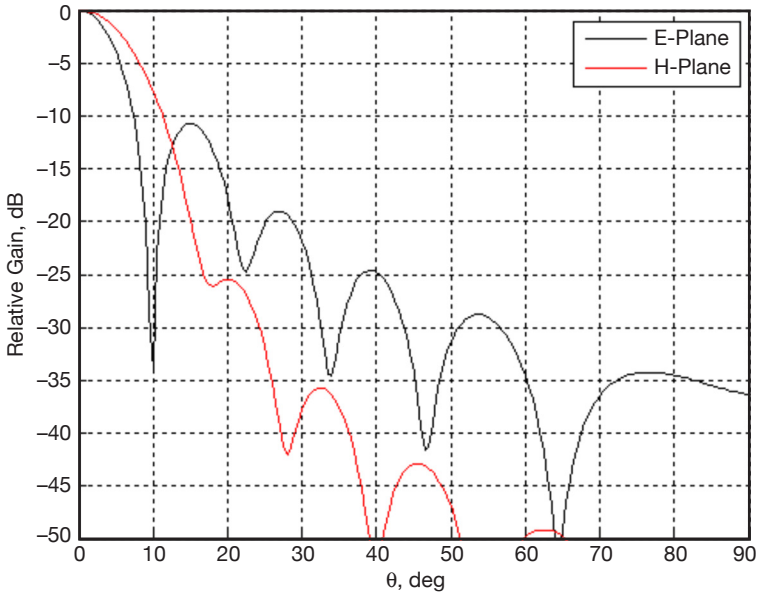

Figure 6. Existing L-band feedhorn pattern at 1.9 GHz.

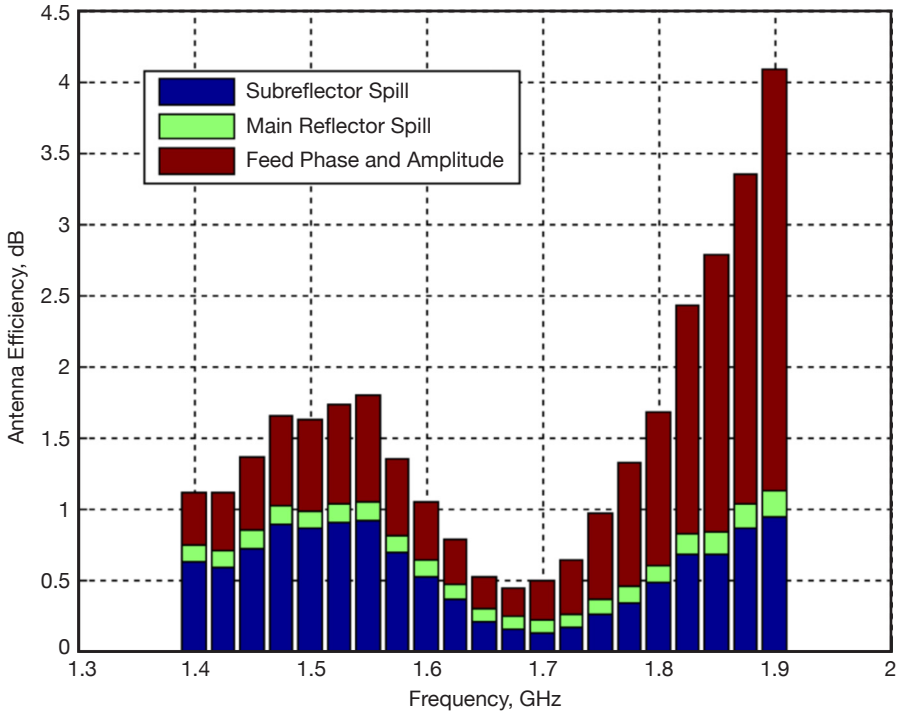

Figure 7. Existing L-band antenna efficiency.

Figure 8 depicts the existing narrowband polarizer design [4]. Here the circular waveguide is deformed in a manner that causes the linearly polarized field with the electric field vector perpendicular to the flattened face to travel with less phase shift than the orthogonal component. The length of this deformation is chosen such that the accumulated phase shift difference between the two orthogonal modes is 90 deg. The device is then excited with equal parts of each linear component by aligning the flat face at 45 deg to the incident linear polarization for which perfect LCP or RCP waves exit the device at the design frequency, assuming reflection is negligible. Reflections are kept to a minimum by adding a matching step at each end of the device, visible in Figure 8.

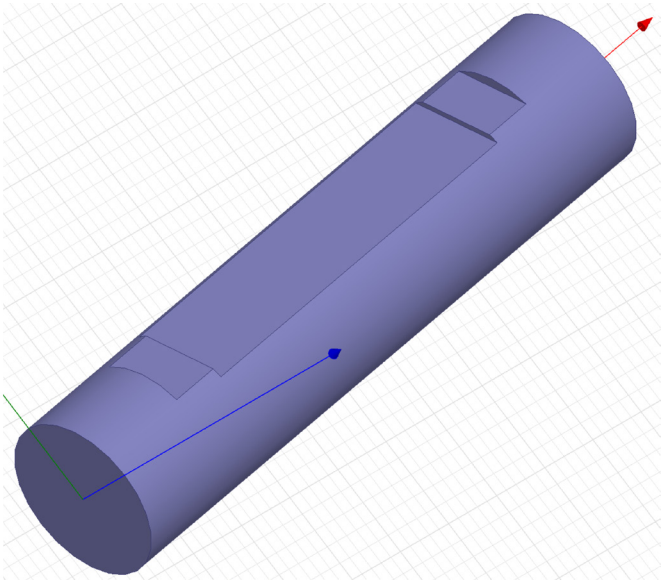

Figure 8. Existing polarizer model.

The performance of the existing polarizer was computed and a summary of the results is given in Figure 9. Note that return loss of the polarizer when fed with a linearly polarized field at 45 deg is negligible at better than 30 dB across nearly the full 1.4–1.9 GHz band. However, the purity of the polarization exiting the device is quite narrowband. A reasonable requirement for the current application is to have the cross-polarized component at least 25 dB below the main polarization. The existing polarizer achieves this level of purity over a range of approximately 0.15 GHz, whereas the broadband requirement is 0.5 GHz. The existing polarizer has nearly a –10 dB cross-polarization level at 1.4 GHz and a –15 dB level at 1.9 GHz, relatively poor performance. This type of stepped polarizer design is limited by the dispersion inherent in the circular waveguide. In the next section, we will describe a broadband polarizer design, a corrugated feed design, and finally a broadband orthomode design, which are suitable for the 1.4–1.9 GHz operating band.

III. New Component Designs

In this section, we discuss the design, fabrication, and measurement of the broadband corrugated feed and polarizer, as well as the design of the OMT. The new feed's RF design is

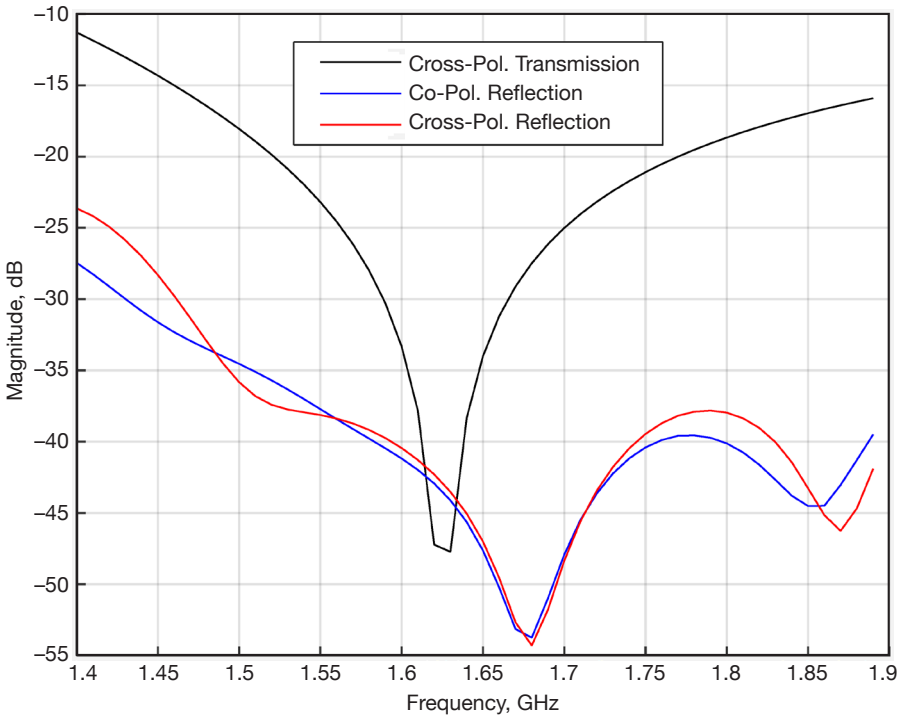

Figure 9. Existing polarizer performance.

straightforward, and mimics the design of many corrugated horns in use throughout the DSN. However, significant effort was put into mechanical design and fabrication of the new feed in order to reduce cost and mass. For the broadband polarizer, a finned diplexer similar to an existing DSN X-band design (7.2–8.5 GHz) was used. The OMT is a more complex component and several different designs are reported in the literature. Complete RF designs for two different versions were completed and the final selection was made considering both RF performance and fabrication cost.

We begin with a discussion of the corrugated horn design. The new corrugated feed must be positioned on the antenna so that its phase center is located in the same position as the original feed. For installation simplicity, we also require that its overall length match the original Potter feed as closely as possible. Figure 10 shows a side view of the new and old feed assemblies, including the horn, polarizer, and spacers. Figure 11 shows a photo of the completed horn assembly in the laboratory.

The RF design of the corrugated horn is quite conventional [5]. For this application, the corrugation period is 1.4 in (35.56 mm), and the width of the fins is 0.15 in (3.81 mm). The small ratio of fin width to corrugation period was chosen to simplify the manufacturing process and reduce mass. The first few corrugations are adjusted in both depth and period in order to optimize the input match of the horn. The final aperture diameter is 35.15 in (892.81 mm). Overall, the feed contains approximately 185 corrugations.

Once fabrication of the components was completed, radiation patterns of the horn were measured on a near-field range. Due to the limitations of the available probe, the lower

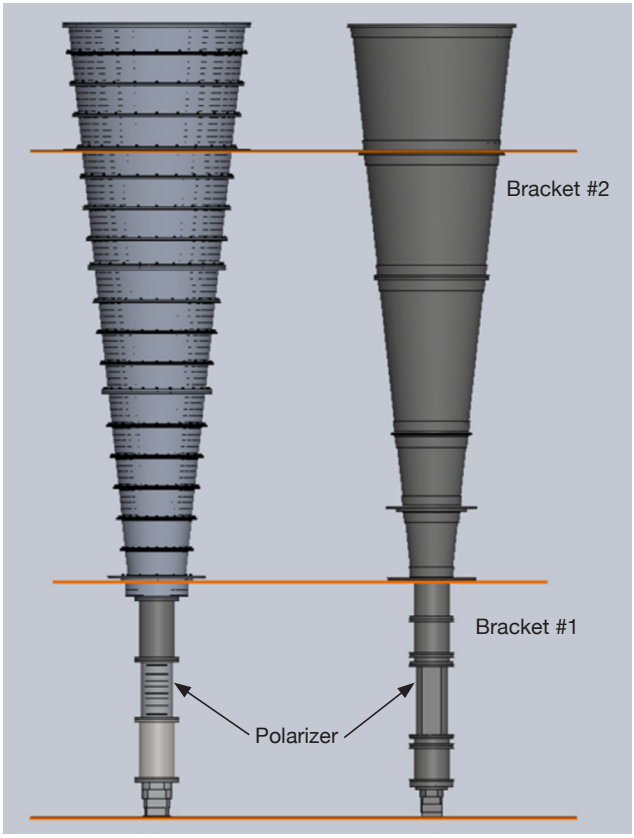

Figure 10. Potter and corrugated horns.

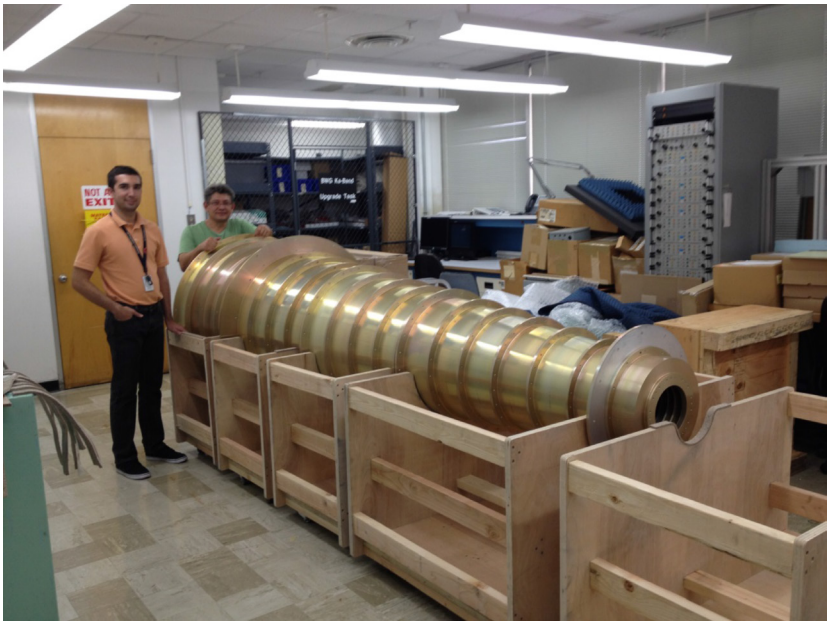

Figure 11. Assembled L-band horn.

frequency limit for the measurements is approximately 1.5 GHz. Figures 12–14 compare the measured and calculated radiation patterns for the feed at 1.518, 1.668, and 1.918 GHz. Because of the low frequencies involved and the limited scan range of the measurement system, we are limited to approximately 40 deg of pattern measurement, with the last 10 deg of that range subject to some truncation error.

The measured patterns are in excellent agreement with the computed results. Excellent pattern symmetry, equal E- and H- plane patterns, and low sidelobes are present at all measured frequencies. This measured data serves to verify the mechanical fidelity of the horn and we expect the performance of the feed on the antenna to match predictions across the entire 1.4–1.9 GHz band.

The input match of the horn is also an important feedhorn parameter, and the computed return loss is shown in Figure 15. An excellent match, with reflections nearly 35 dB below the incident power, is predicted. The reference position for this calculation is at the horn's circular waveguide input. This position is not amenable to calibrated measurements with a network analyzer, which requires a rectangular waveguide port. Later in this section, we will present return loss measurements for the overall feed system, including the horn, polarizer, and a rectangular to circular transition. This measurement is dominated by the auxiliary components whose return loss masks the feed results of Figure 15.

The computed antenna efficiency using the new corrugated horn is shown in Figure 16. These results should be compared to those of Figure 7 for the existing Potter horn. Using the new horn, the loss in efficiency is relatively constant, and approximately equal to the mid-band efficiency for the existing system, across the full 1.4–1.9 GHz operating band. Excellent pattern symmetry is reflected in very low values for the inefficiency due to the feed pattern (red). Spillover past the subreflector is a decreasing function of frequency due to a slight narrowing of the feed's beamwidth over the band. Spillover past the main reflector is also well-controlled across the band.

The mechanical design of the new L-band feed required significant effort, due to the sheer size of the device. With an overall length of over 10 ft (3 m), and a diameter of nearly 3 ft (1 m), this is the largest corrugated feed ever designed, built, and fielded in the DSN. The weight of the horn is approximately 900 lb (400 kg), with an additional 225 lb (102 kg) required for mounting brackets.

Figure 17 shows a CAD model of the completed feed components along with their handling fixture. The overall horn is broken up into four sections plus an input matching section. These sections are each further broken up into four to six slices. Alignment between slices and between sections is accomplished with alignment pins located to within ± 0.025 in (± 0.635 mm). Slices for an individual section are preassembled at the vendor facility for inspection and to verify alignment prior to delivery to JPL. Figure 18 shows a pair of assembled horn sections at JPL and a slice under inspection at the vendor facility.

The fabrication concept of slices and sections allows for optimization of the cost since errors in an individual slice do not cause rejection of a large section of the feed. This allowed the vendor to hold sufficient reserve funding only for errors in an individual slice, a relatively

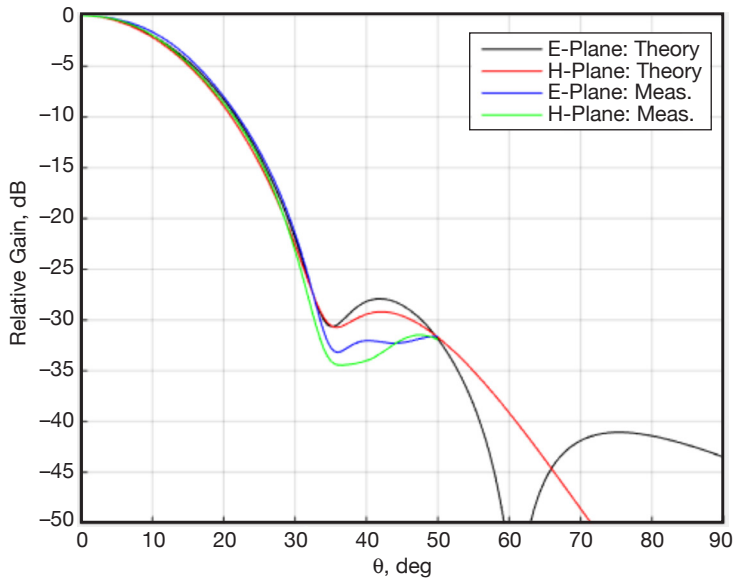

Figure 12. Measured radiation patterns at 1.518 GHz.

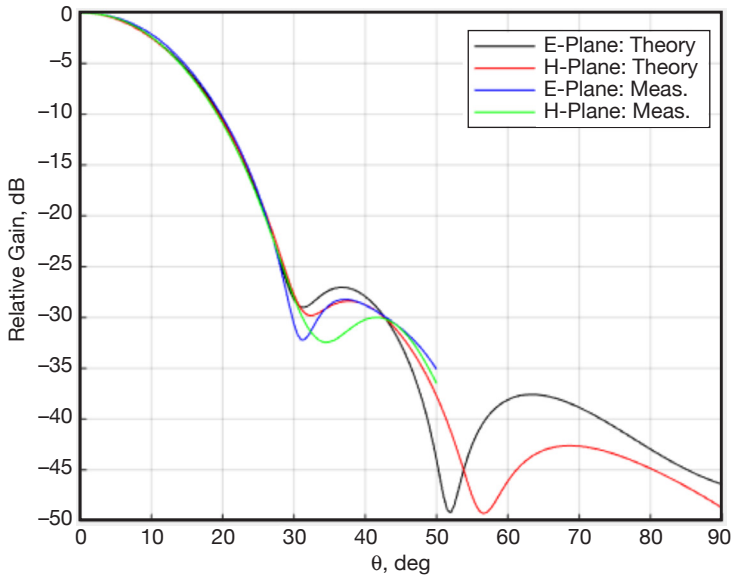

Figure 13. Measured radiation patterns at 1.668 GHz.

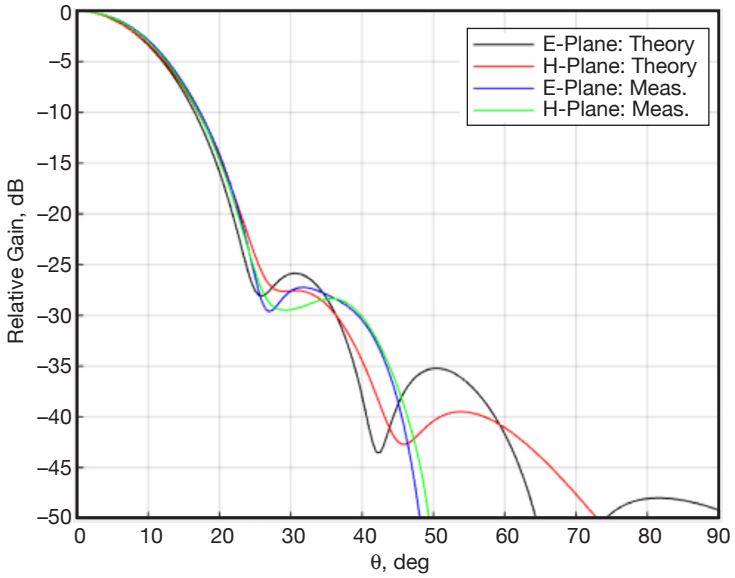

Figure 14. Measured radiation patterns at 1.918 GHz.

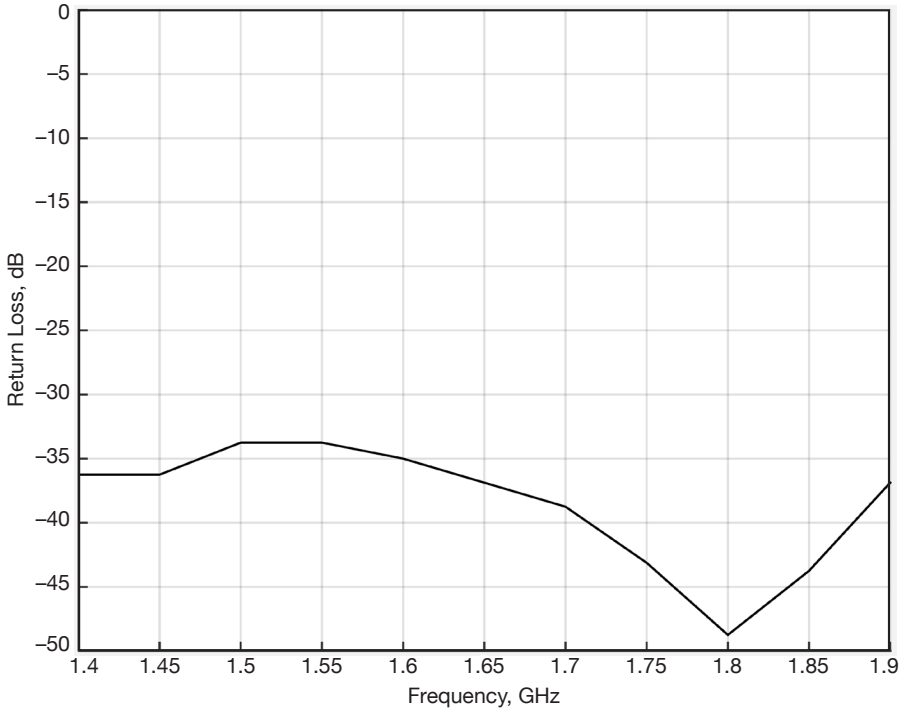

Figure 15. Computed horn return loss.

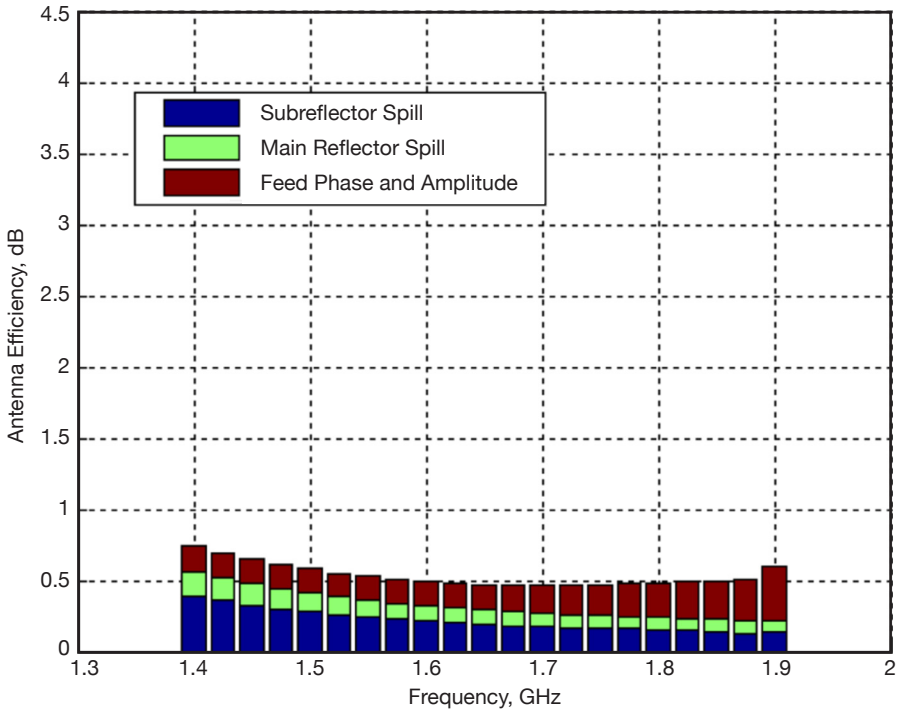

Figure 16. Upgraded L-band antenna efficiency.

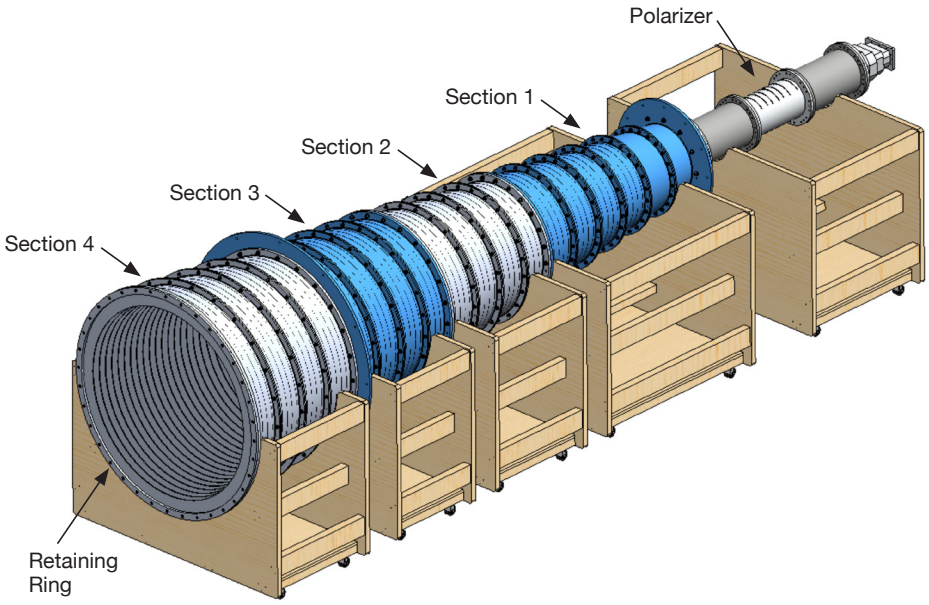

Figure 17. CAD model of feed and fixture.

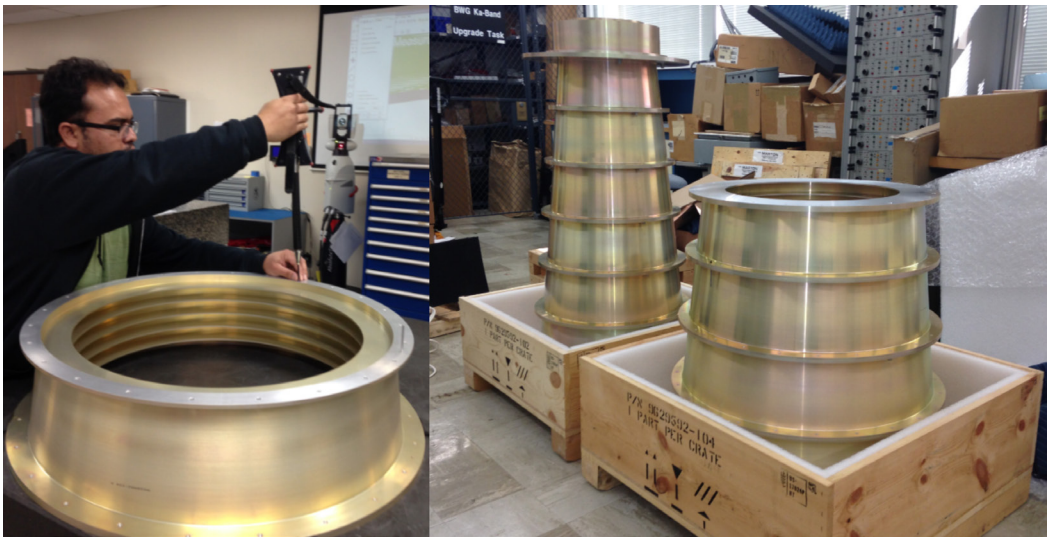

Figure 18. Photo of feed sections and slices.

low-cost part relative to the overall cost of the feed. In addition, tolerances consistent with L-band operation were placed on the feed, ± 0.010 in (± 0.254 mm), which also minimized cost. The decision to use relatively thin fins eased manufacturing difficulty and reduced overall mass.

Next we consider the design of the wideband polarizer. A reasonable performance requirement for this device is that the cross-polarized component generated should be at a level of 25 dB below the co-polarized component. As discussed previously, the existing design would meet this requirement over approximately 0.15 GHz, far less than the 0.5 GHz bandwidth required.

Many different polarizer designs have been developed for various narrowband and wideband applications [6]. The corrugated polarizer (fin type) is an example of a broadband polarizer that has been used in the past for a DSN transmit/receive application at X-band. This particular design has been chosen for the present application due to its compact nature and ease of fabrication.

Figure 19 depicts a CAD model of a corrugated polarizer in a circular waveguide. The basic principle of operation is identical to the existing narrowband device. Fields polarized perpendicular to the fins experience a different phase shift than fields parallel to the fins. The number of fins, profile of the fin depth, and spacing work together to provide a differential phase shift of 90 deg, and a good match for the incident field.

The design was optimized using the commercial mode-match software WASP-NET.[1] This optimization resulted in a symmetrical arrangement of eight fins with variable spacing and depths in a circular waveguide with diameter 6.844 in (173.84 mm). The fin thickness is 0.079 in (2.01 mm), and the maximum fin penetration is approximately 1.0 in (25.4 mm). The overall length of the polarizer is approximately 13.5 in (342.9 mm). Figure 20 is a photograph of the fabricated polarizer, interfaced to the feed for testing on the range.

[1] http://www.mig-germany.com/

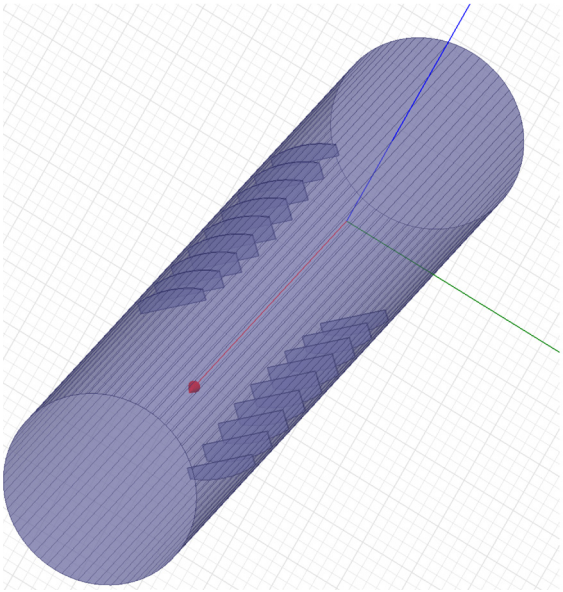

Figure 19. Broadband polarizer model.

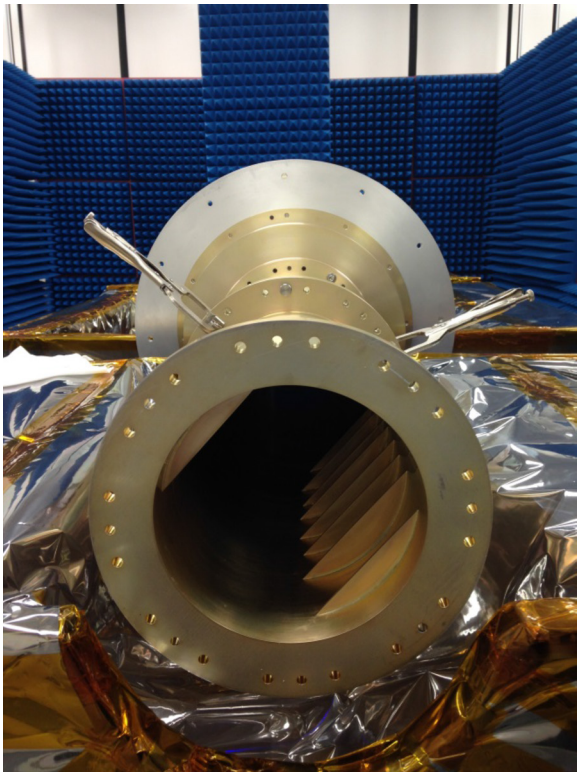

Figure 20. Broadband polarizer.

Figures 21 and 22 show the computed performance of the optimized polarizer. Figure 21 shows the level of co-polarized (RCP) signal exiting the polarizer (black line, at nearly 0 dB across the frequency band coinciding with the top of the plot boundary), and the level of cross-polarized signal (LCP) (red line). The appropriate excitation for RCP is a linearly polarized field oriented at 45 deg relative to the fins. Excitation at –45 deg will generate LCP as the co-polarized component and RCP as cross-polarized radiation in this case. Due to reciprocity, the result for this excitation is that of Figure 21 with the RCP and LCP labels swapped. The result shows better than 35 dB cross-polarization across most of the band, peaking at the design goal of –25 dB at 1.4 GHz.

Figure 22 shows the reflected field magnitudes when the polarizer is excited for RCP. Both components of the reflected field are more than 30 dB below the incident field, which is more than satisfactory.

The performance of the polarizer was measured in the laboratory. One of these polarizers was subsequently mated to the horn and the polarization purity was measured once again on the antenna range. For the laboratory measurement, the polarizer was placed between two rectangular to circular transitions and the transmitted magnitude and phase was measured once for the electric field parallel to the fins and once for the field perpendicular to the fins. Ideally, the measured phase difference would be exactly 90 deg and the transmission magnitudes would be identical. Upon measurement of the two transmission coefficients, we then simulate the co-polarized and cross-polarized components exiting the polarizer if it were excited at 45 deg (RCP excitation).

The results of the laboratory measurements and calculation are shown in Figure 23. The data indicate that while the polarizer does not achieve the predicted –35 dB cross-polarization, it does very nearly meet our goal of –25 dB across the band.

In addition, the polarization at the peak of the horn radiation pattern was measured directly on the antenna range at select frequencies, and the results are indicated by red dots in Figure 23. As expected, the directly measured values of polarization are in good agreement with those based on bench measurements of phase shift for the two possible linear excitations, as described above.

For reference, this difference in performance indicates that a differential phase shift of 85 deg was achieved, whereas 88 deg was expected from the optimization. Two polarizers were fabricated, and both units measure approximately the same, which would indicate a small systematic error, either with the initial design or in fabrication. Although the polarizer design is acceptable, we intend to determine the root cause prior to the next polarizer fabrication cycle.

The final laboratory measurement made on the feed system was an overall return loss measurement, which is shown in Figure 24. From 1.45–1.90 GHz, the return loss is less than –25 dB, and it rises sharply at the low end of the band to –15 dB at 1.4 GHz. The sharp rise is primarily a result of WR430 becoming very close to cut-off at the low end of the band, making the design of the rectangular to circular transition very difficult. This issue will be avoided when a fully dual-polarized system is implemented using an OMT. This device is the next topic of discussion.

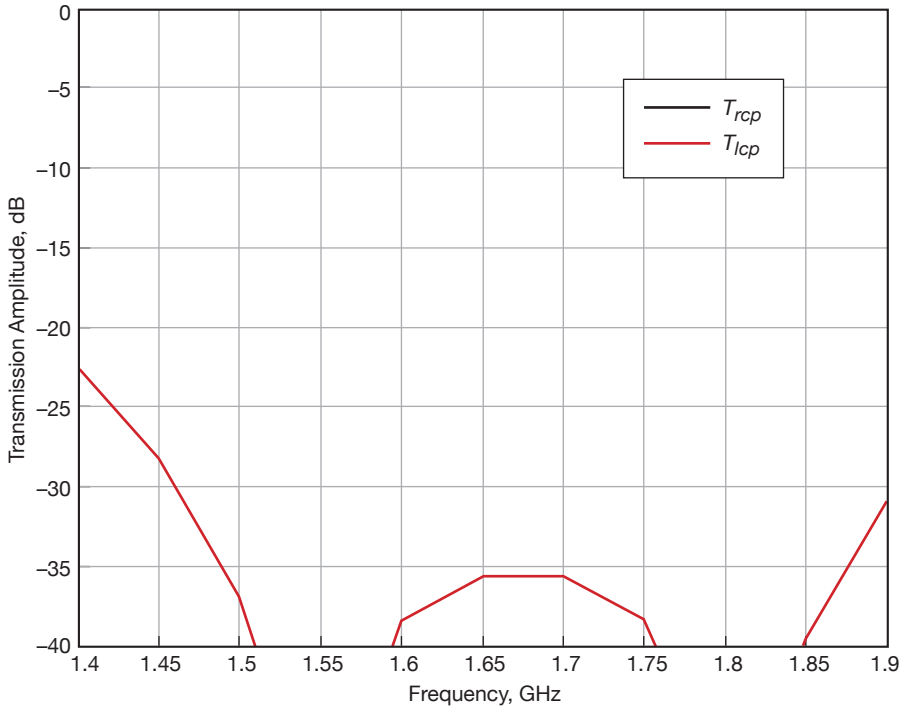

Figure 21. Broadband polarizer cross-polarization.

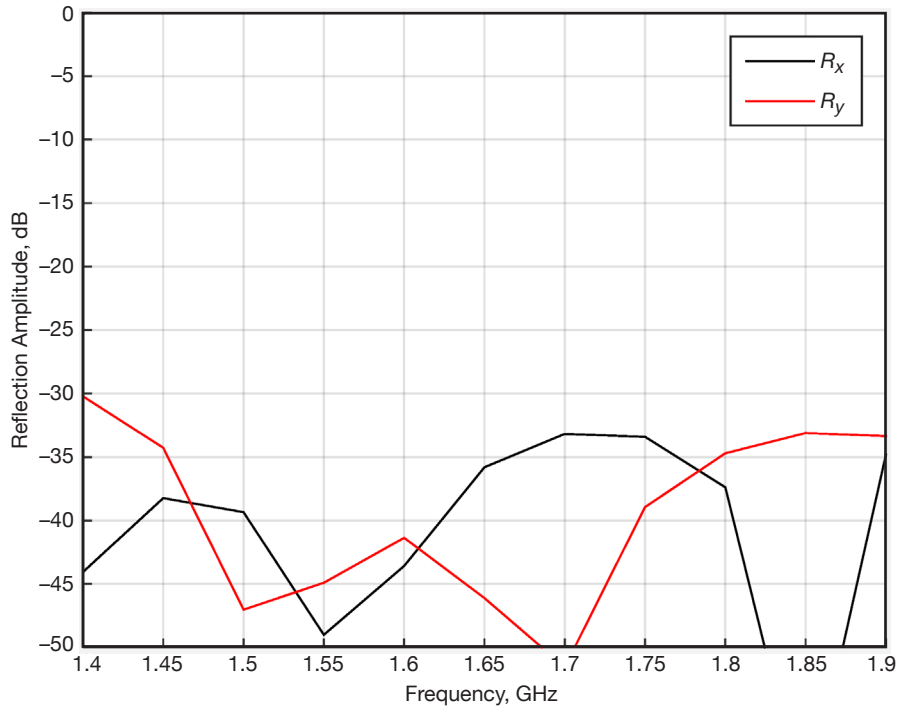

Figure 22. Broadband polarizer return loss.

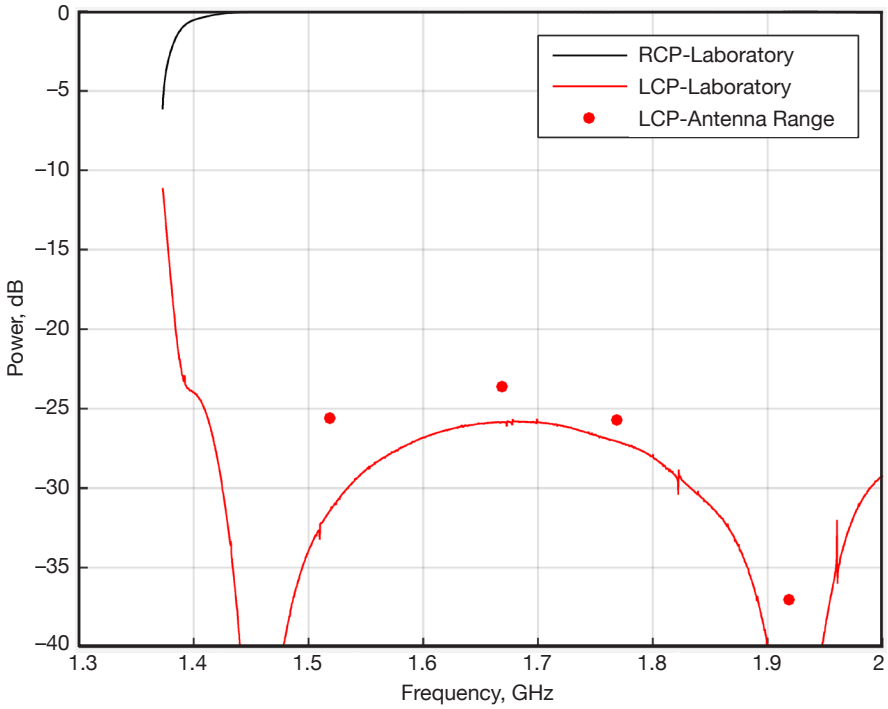

Figure 23. Broadband polarizer measured performance.

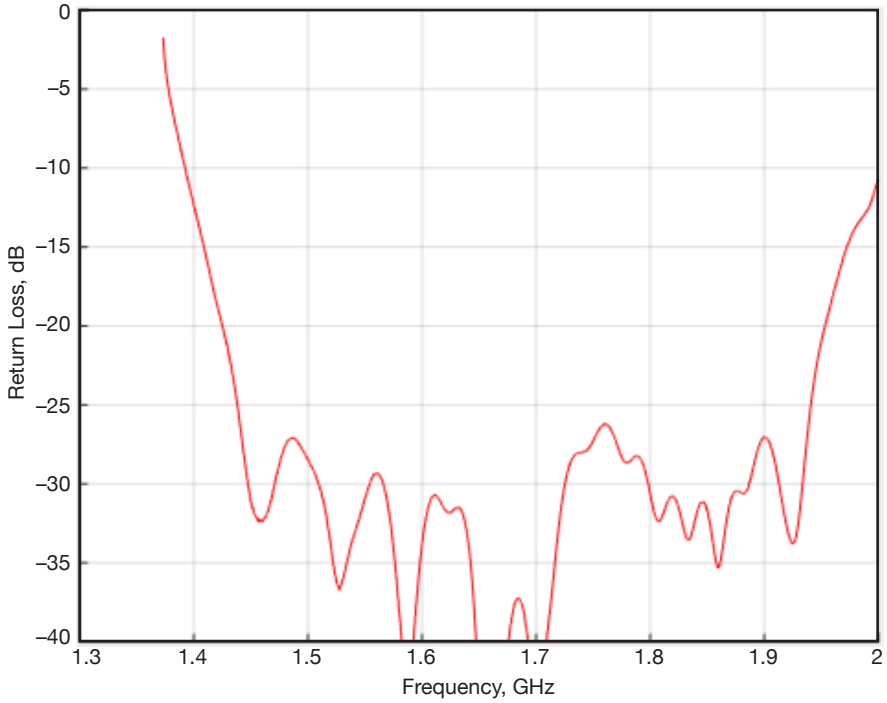

Figure 24. Feed plus polarizer plus waveguide transition return loss measurement.

The final component required to provide a broadband dual-polarization system is an OMT. The OMT provides ports for excitation of two linearly polarized fields in an output circular waveguide. These two linear polarizations are then transformed into RCP and LCP by the polarizer, as described above.

Many different OMT designs are possible [6], and the design effort began with a survey of the available options. The available broadband OMT types included equal dual-junction or turnstile OMT [7], a quad-ridged OMT [8], and a distinct dual-junction OMT [9].

Preliminary RF designs for both the turnstile OMT and the distinct dual-junction OMT were completed. Next, the trade-off between size, fabrication cost, and RF performance was assessed. At the end of this process, the distinct dual-junction solution was deemed superior in terms of form factor, and was chosen for implementation.

Figure 25 shows two views of the CAD model of the OMT. The top view shows the y-polarized WR430 input port (y designated as out of the paper), which is then bent 90 deg and expanded into a square waveguide. The square waveguide is then split with a septum into two stacked ports on the OMT section itself. The septum is visible in the cut-away view at right. The x-polarized WR430 port is at the rear of the device. It is also bent, expanded into a square guide, and then split into two waveguides that feed opposite sides of the OMT in a balanced fashion. This accounts for two more ports on the OMT, and the output square waveguide makes up the fifth port. The square output port of the OMT is than step-transformed into a circular waveguide port compatible with the polarizer.

This L-band OMT is quite large, with an overall length of 55.131 in (1400.33 mm) and a width of 26 in (660.40 mm). The estimated weight of the aluminum OMT is 145 lb (66 kg).

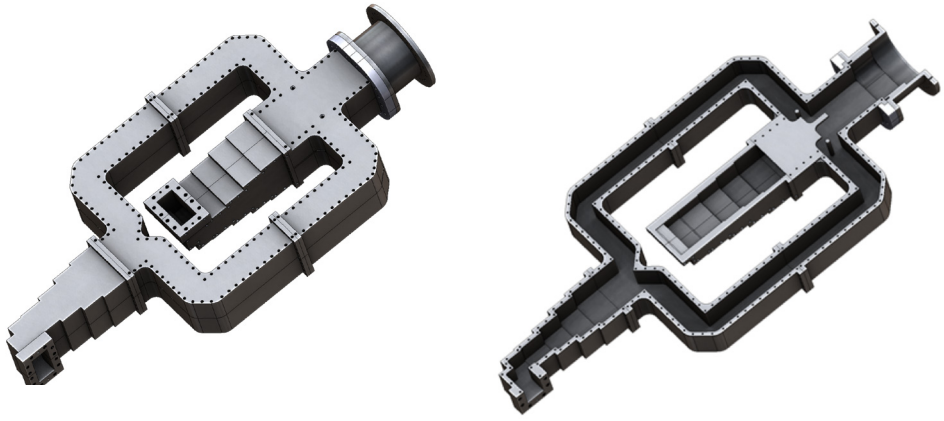

Figure 25. OMT model.

Figure 26 shows the predicted return loss for the OMT's two input ports, WR430. Better than 20 dB return loss is achieved over most of the 1.4–1.9 GHz band for each port. Theoretically, the isolation between ports is infinite due to the symmetry of the device. In practice the isolation will be finite, but large, due to tolerances in fabrication. Typical realized results for this type of device would be in the 40 dB range. The overall cross-polarization for the feed system will be dominated by the polarizer performance itself, at –25 dB from 1.4–1.9 GHz.

The next steps in the OMT development are fabrication and testing of a prototype device. As was mentioned earlier, installation on the antennas will occur in phase two of the upgrade where the broadband single-polarization system with new horn and polarizer and redundant LNAs will be converted to a simultaneous dual-polarization system.

Figure 27 shows a CAD model view of the feed, polarizer, and OMT in the tri-cone area of the 70-m antenna. The two ports that pass through the floor of the tri-cone structure to the RCP and LCP LNAs are also visible in the lower center of the figure. The WR430 waveguides that connect the OMT ports to the LNAs are omitted for clarity in this model.

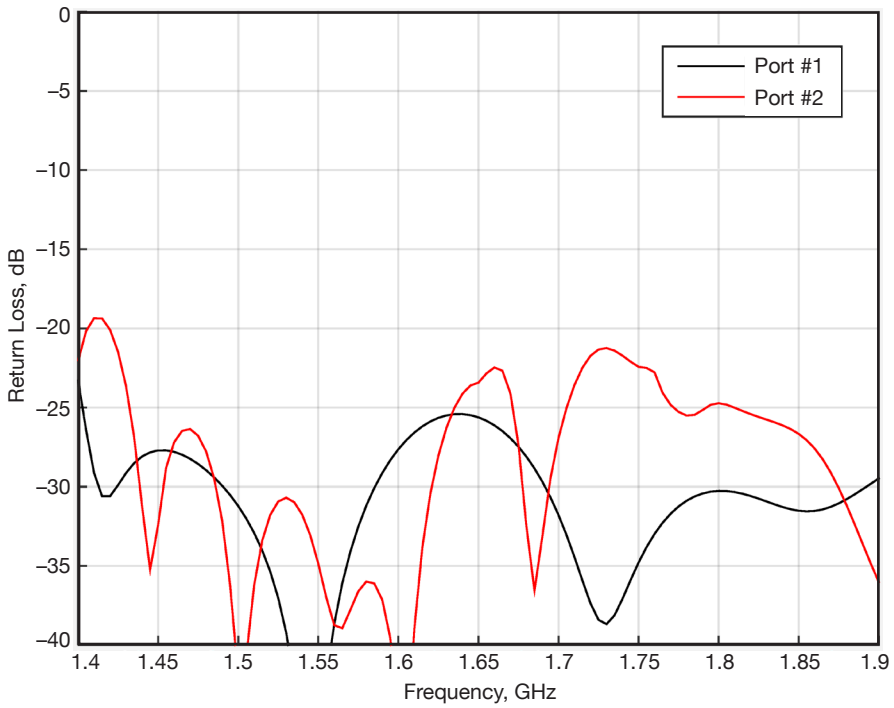

Figure 26. Predicted OMT performance.

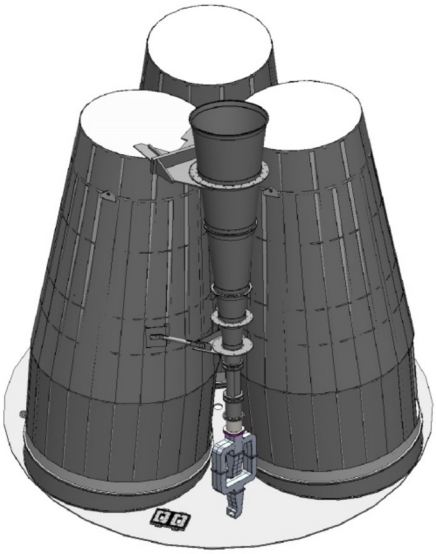

Figure 27. CAD model of L-band feed system on the antenna.

IV. Conclusion

A summary of the new wideband upgrade for the 70-m L-band radio astronomy system has been presented. The new corrugated feed and polarizer have been designed, fabricated, and tested. In the first phase of the installation, the new feed and polarizer will be installed on the 70-m antennas, resulting in a single polarization and wideband operation. Subsequently, the OMT described in this article will be fabricated, tested, and installed, allowing for simultaneous, dual-polarization science observations. Future reports will describe the results of the OMT measurements and characterization of the complete broadband system on the antennas.

Acknowledgment

The authors would like to acknowledge Hungsheng Lin for his expertise in measuring the antenna patterns.

References

[1] J. Withington, "DSN 64-Meter Antenna L-Band (1668-MHz) Microwave System Performance Overview," *The Telecommunications and Data Acquisition Progress Report*, vol. 42-94, Jet Propulsion Laboratory, Pasadena, California, pp. 294–300, April–June 1988, article dated August 15, 1988. http://ipnpr.jpl.nasa.gov/progress_report/42-94/94X.PDF

[2] R. W. Hellings and G. S. Downs, "Upper Limits on the Isotropic Gravitational Radiation Background from Pulsar Timing Analysis," *The Astrophysical Journal*, vol. 265, issue 2, pp. L39–L42, February 15, 1983.

[3] P. D. Potter, "A New Horn Antenna with Suppressed Sidelobes and Equal Beamwidths," JPL Technical Report No. 32-354, Jet Propulsion Laboratory, Pasadena, California, February 25, 1963.

[4] J. R. Pyle, "Cutoff Wavelengths of Waveguides with Unusual Cross Sections (Correspondence)," *IEEE Transactions on Microwave Theory and Techniques*, vol. 12, issue 5, pp. 556–557, September 1964.

[5] P. J. N. Clarricoats and A. D. Olver, *Corrugated Horns for Microwave Antennas*, IEEE Electromagnetic Waves Series, December 1983.

[6] J. Uher, J. Bornemann, and U. Rosenberg, *Waveguide Components for Antenna Feed Systems: Theory and CAD*, Artech House Antenna Library, December 1993.

[7] A. Navarrini and R. L. Plambeck, "A Turnstile Junction Waveguide Orthomode Transducer," *IEEE Transactions on Microwave Theory and Techniques*, vol. 54, no. 1, January 2006.

[8] G. M. Coutts, "Octave Bandwidth Orthomode Transducers for the Expanded Very Large Array," *IEEE Transactions on Antennas and Propagation*, vol. 59, no. 6, June 2011.

[9] G. Narayanan and N. R. Erickson, "A Novel Full Waveguide Band Orthomode Transducer," Thirteenth International Symposium on Space Terahertz Technology, March 2002.